

Electronic structure of ThRu₂Si₂ studied by angle-resolved photoelectron spectroscopy: Elucidating the contribution of U 5*f* states in URu₂Si₂

Shin-ichi Fujimori,¹ Masaaki Kobata,¹ Yukiharu Takeda,¹ Tetsuo Okane,¹ Yuji Saitoh,¹ Atsushi Fujimori,^{1,2} Hiroshi Yamagami,^{1,3} Yuji Matsumoto,^{4,*} Etsuji Yamamoto,⁴ Naoyuki Tateiwa,⁴ and Yoshinori Haga⁴

¹Materials Sciences Research Center, Japan Atomic Energy Agency, Sayo, Hyogo 679-5148, Japan

²Department of Physics, University of Tokyo, Hongo, Tokyo 113-0033, Japan

³Department of Physics, Faculty of Science, Kyoto Sangyo University, Kyoto 603-8555, Japan

⁴Advanced Science Research Center, Japan Atomic Energy Agency, Tokai, Ibaraki 319-1195, Japan

(Dated: August 3, 2022)

The electronic structure of ThRu₂Si₂ was studied by angle-resolved photoelectron spectroscopy (ARPES) with incident photon energies of $h\nu = 655\text{--}745$ eV. Detailed band structure and the three-dimensional shapes of Fermi surfaces were derived experimentally, and their characteristic features were mostly explained by means of band structure calculations based on the density functional theory. Comparison of the experimental ARPES spectra of ThRu₂Si₂ with those of URu₂Si₂ shows that they have considerably different spectral profiles particularly in the energy range of 1 eV from the Fermi level, suggesting that U 5*f* states are substantially hybridized in these bands. The relationship between the ARPES spectra of URu₂Si₂ and ThRu₂Si₂ is very different from the one between the ARPES spectra of CeRu₂Si₂ and LaRu₂Si₂, where the intrinsic difference in their spectra is limited only in the very vicinity of the Fermi energy. The present result suggests that the U 5*f* electrons in URu₂Si₂ have strong hybridization with ligand states and have an essentially itinerant character.

PACS numbers: 79.60.-i, 71.27.+a, 71.18.+y

I. INTRODUCTION

Compounds with AB_2X_2 stoichiometry and the ThCr₂Si₂-type crystal structure, abbreviated as “122” compounds, exhibit a rich variety of physical properties. They consist of the alternating stacks of quasi-two-dimensional *A* and *B*₂*X*₂ layers, resulting in peculiar physical properties in this series of compounds [1]. In recent years, iron-based superconductors with this crystal structure have been found [2]. Furthermore, heavy fermion compounds such as CeCu₂Si₂ [3], CeRu₂Si₂ [4], and YbRh₂Si₂ [5] have the same crystal structure. In particular, these heavy fermion compounds have been attracting much attentions due to their proximity to the quantum critical point [6, 7].

In this class of materials, URu₂Si₂ holds a unique position owing to its enigmatic hidden order (HO) transition at $T_{\text{HO}} = 17.5$ K [8]. Its order parameter has not been identified in spite of extensive studies with various experimental and theoretical techniques for more than thirty years [9, 10]. A number of angle-resolved photoelectron spectroscopy (ARPES) studies on URu₂Si₂ have been also performed, particularly after the discovery of the spectral change at the HO transition observed by Santander-Syro *et al.* [11]. Although a few common perceptions are shared among those studies, there remains unresolved issues [12–14]. In particular, the role of U 5*f* electrons in URu₂Si₂ remains under extensive debate. In this regard, an understanding of the electronic structure of the non-*f* electron analog ThRu₂Si₂ is essential to further comprehend the electronic structure of URu₂Si₂ and other compounds with the same crystal structure.

In the present paper, we report an ARPES study of

ThRu₂Si₂ using soft x-ray synchrotron radiation ($h\nu = 665\text{--}735$ eV). The detailed band structure and Fermi surfaces of ThRu₂Si₂ were derived experimentally, and they are compared with the result of band structure calculation and the result of URu₂Si₂. It is shown that they were well explained by the band structure calculation based on the local density approximation. Furthermore, the ARPES spectral profiles of ThRu₂Si₂ are considerably different from those of URu₂Si₂, suggesting that U 5*f* states are strongly hybridized in URu₂Si₂.

Denlinger *et al.* first reported an ARPES study of ThRu₂Si₂, in which the band structure and Fermi surface map of ThRu₂Si₂ were obtained with incident photon energies of $h\nu = 17$ and 31 eV [15]. Although overall agreement between the experimental data and the band structure calculation was suggested, the detailed structure of the Fermi surface and band structure were not understood. Meanwhile, dHvA experiments on ThRu₂Si₂ [16, 17] and its diluted alloy U_{0.03}Th_{0.97}Ru₂Si₂ [18] have been reported, and most of the observed branches were well explained by band structure calculations. However, the band structure and the location of each Fermi surface have been not understood yet. They are particularly important information from the view point of comparing results between ThRu₂Si₂ and URu₂Si₂.

Here, note that ThRu₂Si₂ is an archetypal compound of the R^{4+} ($R =$ rare earth or actinide element) state with the ThCr₂Si₂-type crystal structure [19] while a similar non-*f* compound LaRu₂Si₂ has the La³⁺ state. Therefore, a comparison of the electronic structure of this class of materials with ThRu₂Si₂ and LaRu₂Si₂ will provide good criteria to understand the valency of the rare-earth or the actinide element. Another interesting

aspect of studying ThRu_2Si_2 is that the electronic structures, including the topology of Fermi surface, of the materials in this class have certain similarities owing to their quasi-two-dimensional crystal structures. Thus an understanding of the electronic structure of ThRu_2Si_2 is important for further understanding compounds with the same crystal structure.

II. EXPERIMENTAL PROCEDURES

Photoemission experiments were performed at the soft X-ray beamline BL23SU in SPring-8 [20, 21]. The overall energy resolution in angle-integrated photoemission (AIPES) experiments at $h\nu = 800$ eV was about 140 meV, and that in ARPES experiments at $h\nu = 655 - 745$ eV was 90–115 meV, depending on the photon energies. The angular resolution of the ARPES experiments was about $\pm 0.15^\circ$, which corresponds to the momentum resolution of about 0.073 \AA^{-1} at $h\nu = 735$ eV. High quality single crystals of ThRu_2Si_2 were grown by the Czochralski pulling method, as described in Ref. [17]. A clean sample surface was obtained by cleaving the samples in a UHV chamber. The present ARPES experiment was performed for the cleaved surface perpendicular to the c axis. Therefore, the scans along the angular directions correspond to the scan within the k_x - k_y plane while the scan along the photon energy corresponds to the scan along the k_z direction.

Note that compounds with the ThCr_2Si_2 -type crystal structure have two types of cleaving surfaces, and each of them has very different photoemission spectral profiles [15, 22]. Although our photoemission experiments are less sensitive to surface electronic structures owing to highly enhanced kinetic energies of photoelectrons, two types of photoemission spectral profiles were certainly observed depending on the location of the cleaved surface. One of them does not show clear periodic structures along the momentum direction and has lower photon energy dependences. This suggests it is contributed by reconstructed surface electronic structures, which have an essentially two-dimensional nature with different periodicity of the Brillouin zone, as is expected from the bulk crystal structure. The other set of spectra shows a clear periodic structure with the Brillouin zone of the bulk crystal structure, and has considerable photon energy dependencies. Therefore, the latter set of spectra is considered as belonging to the bulk electronic structure, and the data presented in the paper pertain to that set.

The vacuum during the course of measurements was typically $< 1 \times 10^{-8}$ Pa, and the sample surfaces were stable for the duration of measurements (1–2 days) because no significant changes were observed in the ARPES spectra during the measurement period. The positions of ARPES cuts were determined by assuming a free-electron final state where the momentum of electron is expressed as

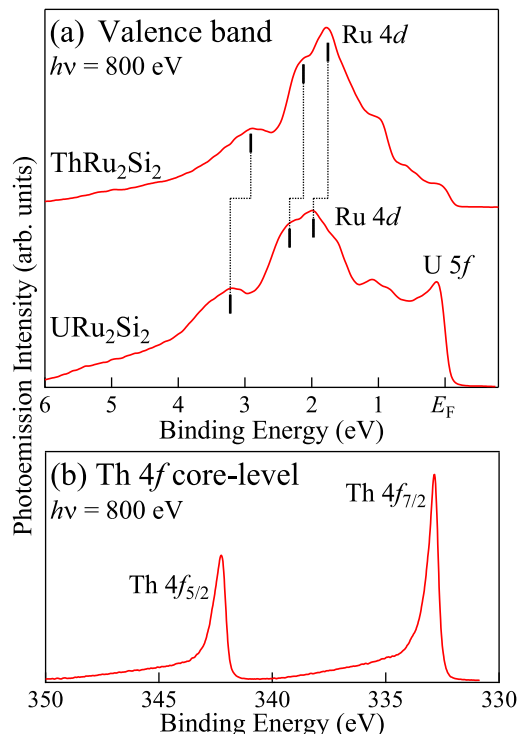


FIG. 1: (Online color) Angle-integrated photoemission spectra of ThRu_2Si_2 measured at $h\nu = 800$ eV. Data of URu_2Si_2 replotted from Ref. [24]. (a) Valence-band spectra of ThRu_2Si_2 and URu_2Si_2 . The locations of pronounced peaks in the Ru 4d bands are indicated. (b) Th 4f core-level spectrum of ThRu_2Si_2 .

$$\begin{aligned}
 k_{\parallel} &= \frac{\sqrt{2mE_{\text{kin}}}}{\hbar} \sin \theta - k_{\parallel\text{photon}}, \\
 k_{\perp} &= \sqrt{\frac{2m}{\hbar^2} (E_{\text{kin}} \cos^2 \theta + V_0)} - k_{\perp\text{photon}} \quad (1)
 \end{aligned}$$

We have taken the inner potential as $V_0 = 12$ eV, which is common value of uranium based compounds [14]. Note that the present ARPES experiment is insensitive to the value of V_0 since E_{kin} is more than one order larger than the inner potential. For ARPES spectra, background contributions from elastically scattered photoelectrons due to surface disorder or phonons were subtracted by assuming momentum-independent spectra. The details of the procedure are described in Ref. [23].

III. RESULTS AND DISCUSSION

A. Angle-integrated photoemission spectra

Figure 1 (a) shows the valence-band angle-integrated photoemission (AIPES) spectra of ThRu_2Si_2 . The spectrum of ThRu_2Si_2 has a complex peak structure. Pronounced peaks located at $E_B \gtrsim 1$ eV originate mainly

from Ru $4d$ states, which do not contribute majorly to the E_F . The AIPES valence-band spectrum of URu_2Si_2 measured at $h\nu = 800$ eV [24] is also shown in the bottom of Fig. 1 (a). The spectrum has a very similar spectral profile to that of ThRu_2Si_2 , except for the state in the vicinity of E_F . The spectrum of URu_2Si_2 contains a sharp peak structure just below E_F , but the structure is absent in the spectrum of ThRu_2Si_2 . This suggests that the specific state in the spectrum of URu_2Si_2 is contributed by U $5f$ states. Interestingly, the locations of pronounced peaks in the Ru $4d$ bands of URu_2Si_2 are located at deeper binding energies by $0.2 - 0.3$ eV than those in ThRu_2Si_2 . This is in contrast with the case of CeRu_2Si_2 and LaRu_2Si_2 where the positions of the Ru $4d$ bands are essentially identical [15]. This suggests that U $5f$ electrons contribute substantially to the valence band as itinerant electrons in URu_2Si_2 , while Ce $4f$ electrons behave almost as core electrons in CeRu_2Si_2 , and they do not majorly influence its valence-band structure.

Figure 1 (b) shows the Th $4f$ core-level spectrum of ThRu_2Si_2 . The spectrum has a relatively simple peak structure with an asymmetric shape having a long tail toward high binding energies. The Th $4f$ core-level spectra of metallic Th compounds are often accompanied by a satellite structure on the high-binding-energy side of $1.4 - 3.1$ eV, and their spectral shapes have been analyzed based on the single impurity Anderson model (SIAM) [25, 26]. The calculations suggest that the intensity of the satellite increases as the DOS at E_F increases. Therefore, absence of the satellite structure in the core-level spectrum of ThRu_2Si_2 is consistent with the almost occupied nature of Ru $4d$ states in this compound. The overall shape of the spectrum is very similar to that of Th metal [27]. This suggests that Th is in the Th^{4+} state although there might be finite contributions from Th $5f$ states in their valence bands [28].

B. Band structure calculation

Before showing the experimental ARPES spectra, the result of band structure calculation in the present study and its relationship to previous studies are summarized. Figure 2 shows the three-dimensional shape of the calculated Fermi surface. Four bands form Fermi surfaces in the band structure calculation. Bands 15 and 16 form small hole-pockets at the Z point. Band 17 forms a large closed Fermi surface centered at the Z point, which is referred to as “pillow.” Its volume is much larger than those of the surfaces formed by bands 15 and 16. Band 18 forms a multiply connected and electron-type Fermi surface, referred to as “jungle-gym.” The total volume of the hole-type and electron-type Fermi surfaces are equal because ThRu_2Si_2 is a compensated metal.

Here, we state the relationship between the present Dirac-type relativistic LAPW calculation with those in Refs. [15] and [17]. The overall topology of the Fermi surface is almost identical to the one in those calcula-

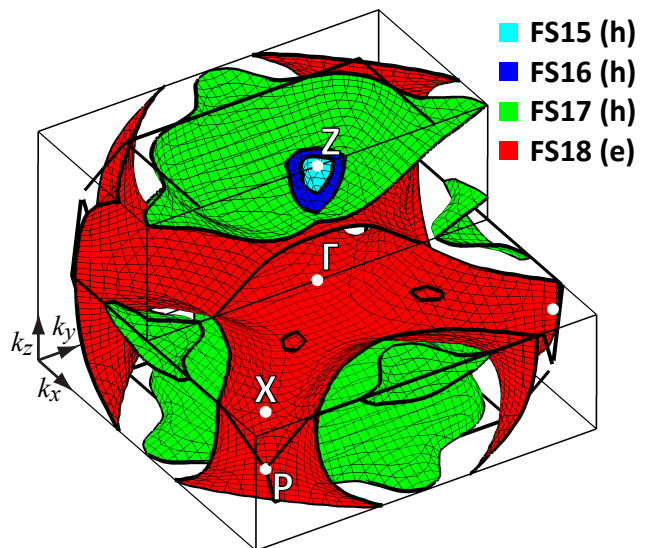


FIG. 2: (Online color) Three-dimensional shape of calculated Fermi surface of ThRu_2Si_2 . Four bands form Fermi surfaces in the calculation. Bands 15 and 16 form small concentric hole-pockets centered at the Z point. Band 17 forms a closed hole-type Fermi surface centered at the Z point, which is referred to as the “pillow.” Band 18 forms a multiply connected electron-type Fermi surface, which is referred to as “jungle-gym” and a small hole-pocket almost in the middle of the Γ -X high-symmetry line. The total volume of the hole-type and the electron-type Fermi surfaces are equal because ThRu_2Si_2 is a compensated metal.

tions, but there are a few minor differences: The topology of the calculated Fermi surfaces in Ref. [15] is identical to the one in the present study, but their sizes and shapes are slightly different. For example, the size of the small Fermi surface located at the center of the Γ -X direction is larger than that derived from the present calculation. This minor difference might be due to improvements in the numerical calculations resulting from significant advances in computational resources, which have enabled us to use a much smaller mesh size. Very similar topology of the calculated Fermi surface was reported in Ref. [17]. One of the major differences between this calculation and the present one is the absence of the electron-type Fermi surface 19 and the existence of the hole-type Fermi surface 15 in the present calculation. These differences originate from the different treatments of lattice parameters and muffin-tin radii in these two sets of calculations. Generally, first-principles band structure calculations based on the density-functional theory include some cutoff parameters which are needed to expand basis functions and potentials, and it is empirically known that energy band dispersions of “122”-type compounds are sensitive to these parameters. In the present calculation, the lattice constants and the muffin-tin radii of potential parameters are optimized by minimizing the total energy, whereas the experimental parameters were used in Ref. [17]. Note that the z parameter, which is

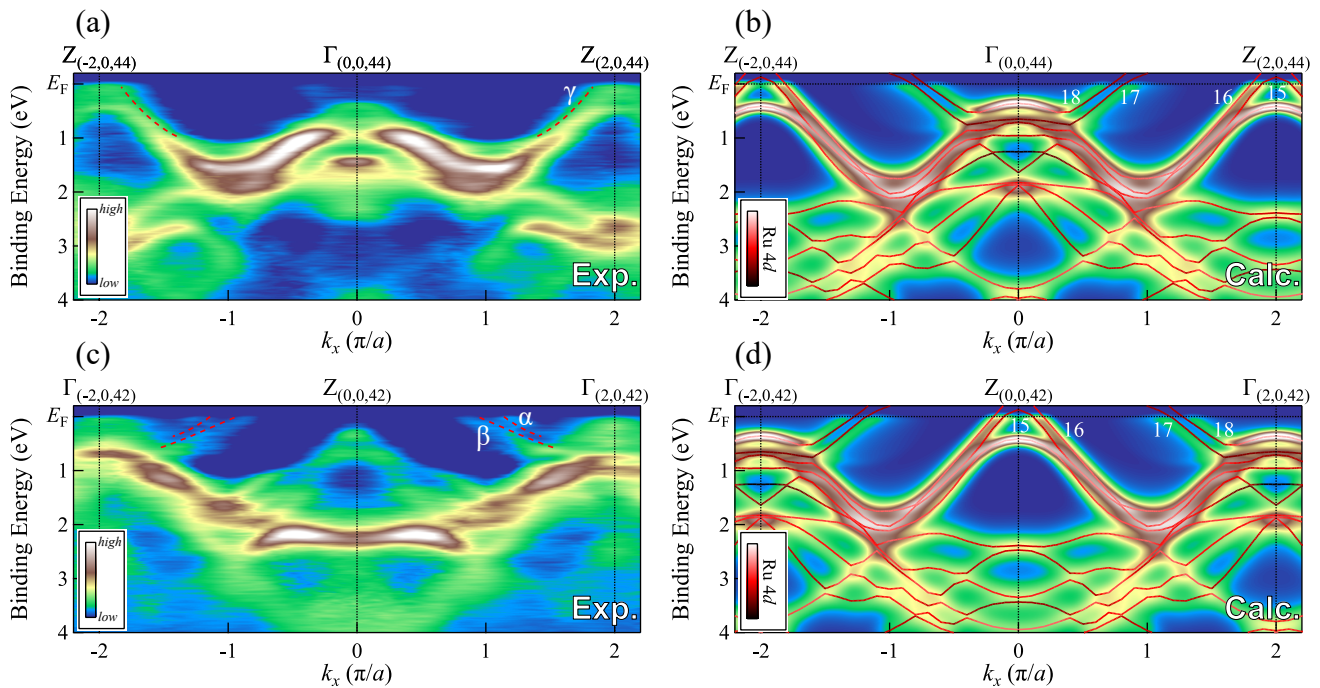


FIG. 3: (Online color) Band structures of ThRu_2Si_2 obtained by photon energy scan of ARPES measurement, together with corresponding results of band structure calculation. (a) ARPES spectra measured along the $Z_{(-2,0,44)}-\Gamma_{(0,0,44)}-Z_{(2,0,44)}$ high-symmetry line. The denotation of the point represents the location of the momentum space in the units of (π/a) for k_x and k_y directions and (π/c) for k_z direction, respectively (See Fig. 4 (a)). Approximate location of the band forming Fermi surface is indicated by dashed curves. (b) The corresponding calculated band structure and the simulation of ARPES spectra. (c) ARPES spectra measured along the $\Gamma_{(-2,0,42)}-Z_{(0,0,42)}-\Gamma_{(2,0,42)}$ high-symmetry line. Approximate location of the bands forming the Fermi surface is indicated by the dashed curves. (d) Corresponding calculated band structure and the simulated ARPES spectra.

the z position of Si atom at 4(e) site, was fixed in this procedure. By this procedure, agreement between the experimental and the calculated band structure improved considerably. Therefore, we use the result of this calculation. As we have learned, there are a few inherent issues in band structure calculations, although they have been considered *ab initio* calculations. This matter is outside the scope of the present paper, and their details pertaining to it will be discussed elsewhere.

Interestingly, the overall shape of the Fermi surfaces is very similar to those of the Fermi surface of other rare-earth compounds with the same crystal structure. For example, the renormalized band calculation of YbRh_2Si_2 [29] predicts that there exist similar “pillow” (“donut” in Ref. [29]) and “jungle-gym” Fermi surfaces. Therefore, they seem to be common features of compounds with the same crystal structure, which might be an origin of the unusual properties of the series of compounds.

In the present study, we have simulated the ARPES spectra based on the calculation. In the simulation, the following effects were taken into account: (i) broadening along the k_\perp direction due to finite escape depth of photoelectrons, (ii) lifetime broadening of the photohole, (iii) photoemission cross sections of orbitals, and (iv) energy resolution and angular resolution of the electron an-

alyzer. The broadening along k_\perp direction is taken to be the inverse of the expected escape depth of photoelectrons in the present experiment (15 Å). Life time broadening is assumed to have a linear dependence on $(E - E_F)$ on a wide energy scale as has been observed in Ni metal[30]. We have assumed that it is zero at E_F and 0.5 eV at $E_B = 5$ eV. The experimental energy and momentum resolutions were assumed to be experimental values as described in Sec. II. The details are described in Ref. [31].

C. Electronic structure within k_x-k_z plane

We first show the ARPES spectra measured along k_x-k_z plane, which correspond to scans along the detection angle of photoelectrons and incident photon energy. Figure 3 (a) shows the ARPES spectra measured along the $Z_{(-2,0,44)}-\Gamma_{(0,0,44)}-Z_{(2,0,44)}$ high-symmetry line. Here, the denotation of the point represents the location of the momentum space in the units of (π/a) for k_x and k_y directions and (π/c) for k_z direction, respectively (See Fig. 4 (a)). Note that the spectra correspond to the angular scan with $h\nu \sim 735$ eV, but contain spectra measured at its vicinity photon energies to exactly trace the

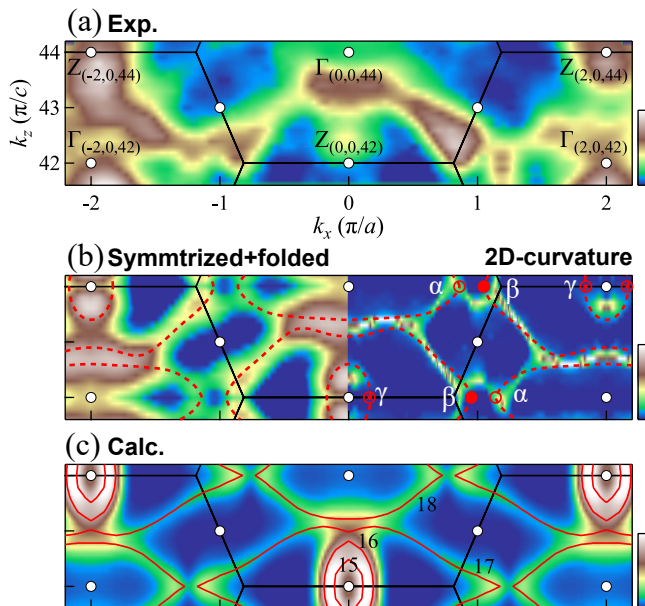


FIG. 4: (Online color) Fermi surfaces of ThRu_2Si_2 obtained by photon energy scan of ARPES measurement, together with corresponding results of band structure calculation. (a) Fermi surfaces of ThRu_2Si_2 obtained by integrating ARPES spectra measured at $h\nu = 655\text{--}745$ eV over 100 meV at E_F . (b) Symmetrized and folded Fermi surface map within the $k_x\text{--}k_z$ plane. The locations of α , β , and γ bands derived from the band structures shown in Fig. 3 (a) and (c) are also indicated by filled circles. Approximate locations of Fermi surfaces derived from the Fermi surface map and the 2D-curvature analysis are indicated by dashed curves. (c) Calculated Fermi surfaces and the simulated Fermi surface map within the $k_x\text{--}k_z$ plane.

high symmetry line according to the Eq. 1. Clear energy dispersions can be recognized. On the higher binding energy side ($E_B \gtrsim 1$ eV), there exist weakly dispersive features with enhanced intensities, which are attributed to bands with the dominant contribution from Ru $4d$ states. Moreover, there exist rapidly dispersing features in the vicinity of the Fermi energy, and some of them seem to form Fermi surfaces. The hole-shaped dispersion centered at $Z_{(2,0,44)}$ and designated as γ has almost linear energy dispersion toward E_F , suggesting that it forms hole-like Fermi surfaces at the Z point. In addition, an electron-pocket-like feature with very weak intensities is observed at the $\Gamma_{(0,0,44)}$ point. Its structure in the vicinity of E_F is particularly vague, and its nature is not well resolved. There is a similar vague feature in the vicinity of E_F in the ARPES spectra measured along the same high-symmetry line at $h\nu = 17$ eV [15], and its details were not well resolved. One possibility is that this is the surface-related electronic structure because its intensity is highly enhanced in their spectra, which should have enhanced contributions from surface electronic structures.

Figure 3 (b) shows the calculated band structure and the simulation of ARPES spectra based on the band

structure calculation. The solid lines represent the band dispersions, and the intensity map shows the result of the simulation. The color coding of the bands is the projection of the contributions from the Ru $4d$ states. Very complicated band dispersions are expected in this energy region. There are cosine-shaped dispersions with enhanced intensities in the binding energy of $E_B = 0.5\text{--}1.5$ eV, which have large contribution from the Ru $4d$ states. Although their energy dispersions are somewhat larger than those in the experimental ARPES spectra, their essential structure is very similar to that observed in the experiment. In the vicinity of the Z point, there exist hole pockets formed by bands 15 and 16. These two bands are so close in momentum that they cannot be observed separately in the simulated ARPES spectra. Therefore, although the feature is very similar to the experimental spectra, the number of Fermi surfaces in the vicinity of the Z point cannot be distinguished experimentally. Meanwhile, the features corresponding to bands 17 and 18 are not observed clearly in the experimental ARPES spectra.

Figure 3 (c) shows the ARPES spectra measured along the $\Gamma_{(-2,0,42)}\text{--}Z_{(0,0,42)}\text{--}\Gamma_{(2,0,42)}$ high-symmetry line. The spectra correspond to the angular scan with $h\nu \sim 665$ eV. The spectra are essentially very similar to those measured along the $Z_{(-2,0,44)}\text{--}\Gamma_{(0,0,44)}\text{--}Z_{(2,0,44)}$ high-symmetry line shown in Fig. 3 (a), but there are some distinct differences between them. One of the major differences is the existence of clear dispersive features in the middle of the $\Gamma_{(0,0,42)}\text{--}Z_{(2,0,42)}$ high-symmetry line in the vicinity of E_F . There are clear hole-like dispersions around $Z_{(0,0,42)}$ point, which are designated as α and β . They did not appear in the ARPES spectra measured along the $\Gamma_{(-2,0,44)}\text{--}Z_{(0,0,44)}\text{--}\Gamma_{(2,0,44)}$ high-symmetry line. Similar phenomena have been also observed in the ARPES spectra of other uranium compounds [31, 32], and they are considered to have originated from the photoemission structure factor (PSF) effect [33]. This effect seems to be particularly significant in compounds with this type of crystal structure [34]. Therefore, it is quite important to observe multiple locations in the Brillouin zone with different photon energies and detection angles to deduce the entire electronic structure.

Figure 3 (d) shows the corresponding calculated band structure and the simulated ARPES spectra based on the band structure calculation. There exist bands 17 and 18, which form a large electron-like Fermi surface around the Γ point and a large hole-like Fermi surface around the Z point; these structures correspond well to band β and α in the experimental ARPES spectra. Accordingly, the band structure along the $Z\text{--}\Gamma\text{--}Z$ high-symmetry line is essentially explained by the band structure calculation although the number of small Fermi surface around Z point could not be resolved in the present experiment.

Next, we discuss the shapes of the Fermi surfaces obtained by these measurements. Figure 4 (a) shows the Fermi surface map along the $k_x\text{--}k_z$ plane obtained by integrating ARPES spectra measured at $h\nu = 655\text{--}745$ eV

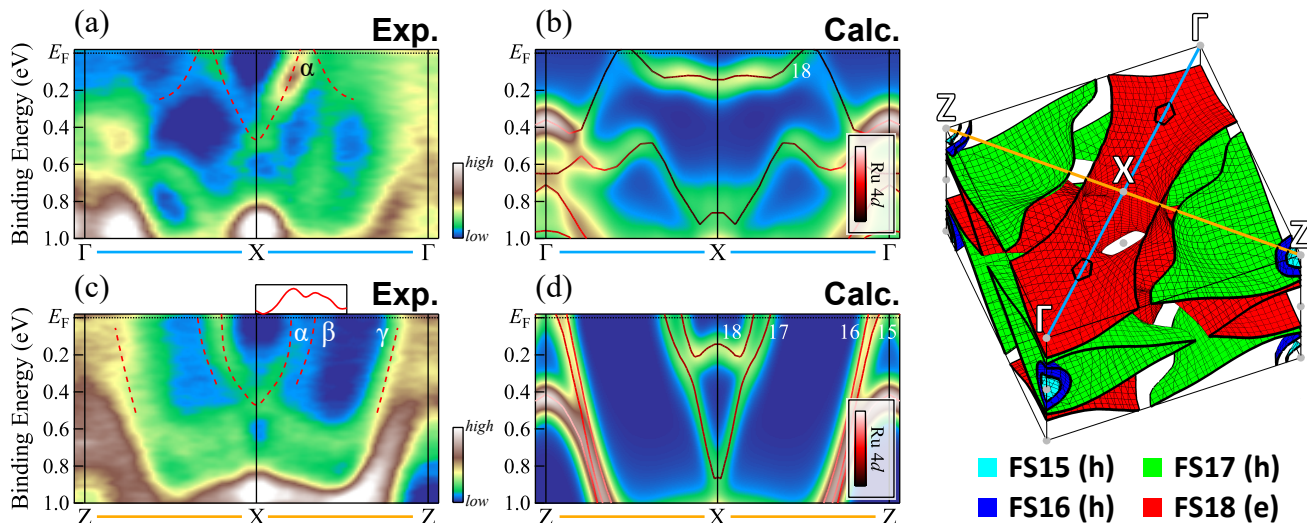


FIG. 5: (Online color) Band structures of ThRu_2Si_2 obtained by angular scan of ARPES spectra measured at $h\nu = 735$ eV, together with the corresponding results of the band structure calculation. (a) ARPES spectra measured along the Γ -X- Γ high-symmetry line. Approximate band location is indicated by the dashed curve α , which forms a small hole-pocket along the path from the X point to the Γ point. (b) Corresponding calculated band structure and the simulated of ARPES spectra. (c) ARPES spectra measured along the Z-X-Z high-symmetry line. Approximate locations of the two bands are designated by the dashed curves α , β , and γ . The upper panel shows the MDC spectrum at E_F . (d) The corresponding calculated band structure and the simulated ARPES spectra. Three-dimensional shape of calculated Fermi surface within the Γ -Z-X plane is also shown.

with 5 eV step over 100 meV at E_F . In this Fermi surface map, the momenta parallel and perpendicular to the surface were calculated based on Eq. 1. The Fermi surface map has complex features. Note that locations with the same symmetry in the Brillouin zone but with different values of k_x and k_z have different profiles. For example, there exists the feature with an enhanced intensity centered at the $Z_{(0,0,42)}$ point ranging over $k_x = -1 - 1(\pi/a)$ and $k_z = 42 - 43.5(\pi/c)$, but the corresponding features are very vague around the $Z_{(\pm 2,0,44)}$ points. Another example is a vertically long ellipsoidal feature centered at the $Z_{(\pm 2,0,44)}$ points, but the intensity of the feature is very weak at the $Z_{(0,0,42)}$ point. Furthermore, there are enhanced intensities in the vicinity of the $\Gamma_{(\pm 2,0,42)}$ points, but there is no corresponding feature in the vicinity of $\Gamma_{(0,0,44)}$ point. They are considered as the contributions from PSF effect as already shown in the band structures shown in Fig. 3.

To avoid the influence from this effect, we have symmetrized and folded the Fermi surface map within the momentum region of $k_x = -2 - 2(\pi/a)$ and $k_z = 42 - 44(\pi/c)$. The left panel of Fig. 4 (b) shows the symmetrized and folded Fermi surface map. The shapes of some Fermi surfaces are well recognized in this intensity map. We have further analyzed this Fermi surface map by using the 2D-curvature method [35], and the result is shown in the right panel of Fig. 4 (b). The locations of α , β , and γ bands derived from the band structures shown in Fig. 3 (a) and (c) are also indicated by filled circles. The approximate shapes of the Fermi surfaces deduced from the Fermi surface map and the 2D-curvature anal-

ysis are indicated by dashed curves. According to these images, there are one large Fermi surface centered at the Γ point designated as α and two Fermi surfaces centered at the Z point designated as β and γ .

We compare these experimental Fermi surfaces with the result of the band structure calculation. Figure 4 (c) shows the Fermi surface obtained by the band structure calculation and the simulated Fermi surface map based on the band structure calculation. Within this high-symmetry plane, there exist four Fermi surfaces formed by bands 15–18. Bands 15 and 16 form small football-shaped Fermi surfaces centered at the Z point. Band 17 appears as the cross-section of the “pillow-shaped” Fermi surface, and it has a horizontally long ellipsoidal shape. Band 18 appears as an electron Fermi surface with a horizontally-long ellipsoidal shape, which corresponds to the horizontal joint of the “jungle-gym” Fermi surface. A comparison between the experimental Fermi surface map and the calculation result suggests that there are certain correspondences between them. For example, the shape of the horizontally long large Fermi surfaces α and β in the experimental Fermi surface map correspond well to the Fermi surfaces of bands 18 and 17, respectively. Furthermore, the vertically long ellipsoid feature around the $Z_{(2,0,44)}$, designated as γ , also corresponds to the calculated Fermi surfaces 15 and 16. On other other hand, there are some disagreements between the experimental and the calculated Fermi surface map. For example, there is an enhanced intensity around the Γ point in the experimental Fermi surface maps although there is no corresponding features in the calculation. This might be

due to the contribution from a surface state as discussed in Fig. 3 (a), but its origin is not clear.

Accordingly, the band structures in the vicinity of the Fermi energy and the topologies of Fermi surfaces within the $k_x - k_z$ plane are qualitatively described by the band structure calculation. The topologies of the football-shaped Fermi surfaces around the Z point and the large Fermi surfaces formed by bands 17 and 18 around the Z and the Γ points agrees with those obtained by band structure calculation although the number of small hole pocket in the very vicinity of the Z point is not well resolved in the present spectra.

D. Electronic structure within $k_x - k_y$ plane

To further understand the shapes of the Fermi surfaces, we have measured ARPES spectra within the $k_x - k_y$ plane. First, we focus on the electronic structure around the X point. Figure 5 (a) shows ARPES spectra of ThRu₂Si₂ measured along the Γ -X- Γ high-symmetry line. These spectra were measured at $h\nu = 735$ eV, which correspond to the ARPES cut with $k_z \sim 44(\pi/a)$. There is a parabolic energy dispersion centered at the X point, whose approximate location is indicated by the dashed curves in the figure as band α . It forms a small hole pocket in between the X and the Γ points. Figure 5 (b) displays the calculated band dispersion and the simulated ARPES spectra. In the calculation, band 18 also forms a small electron pocket in between the X and the Γ points, and its behavior is very similar to the experimentally observed band α , although its momentum position and band width are somewhat different.

Figure 5 (c) shows the experimental ARPES spectra measured along the Z-X-Z high-symmetry line, which is perpendicular to the Γ -X- Γ high-symmetry line. The momentum distribution curve (MDC) at E_F is also shown in the upper panel. The structure around the X point is very similar to that of Γ -X- Γ high-symmetry line, but there exist two bands α and β , that cross the Fermi energy. The existence of the bands α and β can be understood from the MDC spectrum at E_F where two peaks exist in this region. The band β is missing in the left half of the ARPES spectra probably due to the PSF effects. The band structure calculation shown in Fig. 5 (d) also predicts two electron-like bands 17 and 18 centered at the X point which form Fermi surfaces. Their structures in the vicinity of E_F are very similar to the experimental bands β and α in Fig. 5 (c) although their band widths are different. Therefore, although there are some quantitative differences, the essential topology of Fermi surfaces around the X point agrees well with the band structure calculation.

Next, we show the Fermi surface map within the $k_x - k_y$ high symmetry plane to further understand the overall in-plane shape of the Fermi surfaces. Figure 6 (a) shows the Fermi surface map measured along the $k_x - k_y$ plane obtained by integrating at E_F of the ARPES spec-

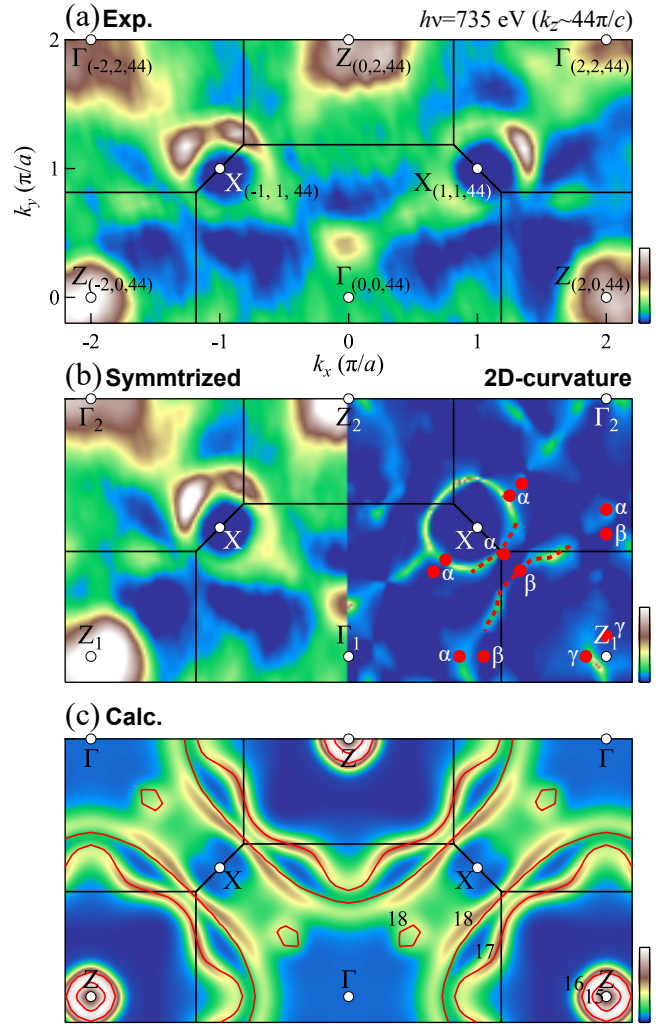


FIG. 6: (Online color) Fermi surfaces of ThRu₂Si₂ obtained by angular scan of ARPES spectra measured at $h\nu = 735$ eV, together with the corresponding results of the band structure calculation. (a) Fermi surfaces of ThRu₂Si₂ obtained by integrating ARPES spectra over 100 meV around E_F . (b) Fermi surfaces of ThRu₂Si₂ symmetrized relative to $k_x = 0$ (right panel) and Fermi surface obtained by the 2D curvature method [35] (left panel). The Fermi momenta deduced from ARPES spectra shown in Figs. 3 and Figs. 5 are plotted by filled circles. Dashed curves are guide to eyes. (c) Calculated Fermi surfaces and the simulated Fermi surfaces within the $k_x - k_y$ plane.

tra measured at $h\nu = 735$ eV over 100 meV. There are a few characteristic features in the Fermi surface map. The most prominent one is the circular-shaped enhanced intensity centered at the X point, which was also observed in the previous ARPES study with $h\nu = 17$ and 30 eV [15]. There is also an enhanced intensity in the vicinity of the Z point, which corresponds to the hole-pocket-like features γ observed in the ARPES spectra shown in Fig. 3 (a). There exist complex features around the Γ point, and its appearance is considerably different between the

$\Gamma_{(0,0,44)}$ and the $\Gamma_{(\pm 2,2,44)}$ points.

To further reveal the in-plane Fermi surface topology, we have symmetrized the Fermi surface map relative to $k_x = 0$, and made its 2D-curvature analysis as shown in the left and right panels of Fig. 6 (b). The Fermi momenta estimated from ARPES spectra measured along the Γ -Z- Γ (Figs. 3 (c)), the Γ -X- Γ (Fig. 5 (a)), and the Z-X-Z (Fig. 5 (c)) high-symmetry lines are also plotted by filled circles. In the result of the 2D-curvature analysis, there is an arc-shaped feature in between the Z₁ and the X points, which corresponds to the part of a hole-type Fermi surface formed by band β centered at the Z point. Although the feature around the X point has a circular shape, the behaviors of the bands α forming this feature are different between the X- Γ and the X-Z directions; it forms a small hole-pocket along the X- Γ direction while two bands α and β form electron-type Fermi surfaces around the X point as shown in Fig. 5(a) and (c). Furthermore, band α forms Fermi surface along the Γ -Z direction, and how they are connected within the plane was not well understood since its intensity is missing in many part of the Brillouin zone. There are complex features around the Γ_1 and the Γ_2 points, but their appearances are considerably different each other. In the symmetrized map, there are enhanced intensities around Γ_2 point, but there is no corresponding feature around the Γ_1 point. The 2D-curvature map also exhibit complex features around these points, but we could not understand the nature of Fermi surface. One possibility is that they might be the contributions from surface states as finite intensities were observed around the Γ point shown in Fig. 3 (a).

The topology of the Fermi surface was not well resolved from the experimental Fermi surface map, and we consider it with the comparison with the result of the band structure calculation. Figure 6 (c) shows the Fermi surface and the simulated Fermi surface map based on the band structure calculation. There exist two concentric hole pockets formed by bands 15 and 16, and the cross-section of the ‘‘pillow’’ formed by band 17 centered at the Z point. Band 18 forms a large open Fermi surface and a small hole-pocket between the Γ and the X points. A comparison between the experimental results and the calculation suggests that there are similar features. For example, there are enhanced intensities around the Z point in both the experimental and the calculated Fermi surface map, which originate from the hole-like Fermi surface around the Z point. In addition, the Fermi surface formed by band β has a very similar topology to the calculated Fermi surface formed by band 17. The Fermi surfaces formed by band α have some common features with the calculated Fermi surface formed by band 18; it forms a small hole-pocket along the Γ -X high symmetry line and large hole-like Fermi surface centered at Z point. On the other hand, the intensity of band α is missing in many part of the Brillouin zone, and an overall agreement between experimental band α and calculated band 18 was not well understood. Accordingly, there are some

similar features in the experimental and calculated Fermi surface maps and band structure although there are some unexplained features particularly around Γ point.

E. Discussion and comparison with URu₂Si₂

We measured the ARPES spectra of ThRu₂Si₂ within the k_x - k_z and k_x - k_y planes, and the topologies of the Fermi surfaces were mostly explained by the band structure calculation although the in-plane topology of the Fermi surface formed by band α was not clear. Here we discuss the relationship between the present result and dHvA studies. In general, the locations of Fermi surface in Brillouin zone cannot be determine by the dHvA, but the size of Fermi surface determined by the ARPES experiment is not as accurate as the one obtained by dHvA experiment owing to various contributions such as instrumental energy resolution, momentum resolution, and the broadening along k_\perp direction [37]. In the dHvA studies by Matsumoto *et al.* [17], branches from three Fermi surfaces α , β , and γ were observed, which correspond to the Fermi surfaces α , β , and γ observed in the present ARPES measurement, respectively. Thus, the result of the present ARPES study is consistent with the dHvA studies concerning the number of Fermi surfaces. Furthermore, the locations of the Fermi surfaces formed by bands β and γ in the Brillouin zone were determined by the present study, and they were consistent with the result of the band structure calculation. Although the topology of the in-plane Fermi surface formed by band α was not completely determined from the present ARPES spectra, the branch α is in the dHvA study was well explained by the band structure calculation, suggesting the topology of Fermi surface α also can be explained by the band structure calculation. Therefore, by combining the results of the ARPES and dHvA studies, it is concluded that the topology of the Fermi surface of ThRu₂Si₂ is mostly explained by the band structure calculation.

Finally, we compare the present result with the ARPES study of URu₂Si₂. Figures 7 (a) and (b) show the ARPES spectra of ThRu₂Si₂ and URu₂Si₂ measured along the X - Γ - Z - X high-symmetry line. The photon energies used were $h\nu = 735$ eV for ThRu₂Si₂ and $h\nu = 760$ eV for URu₂Si₂, which correspond to the ARPES cut with $k_z \sim 44(\pi/c)$. Therefore, the inequalities originating from PSF effects between the ARPES spectra of ThRu₂Si₂ and URu₂Si₂ are absent in the comparison although the slightly different photoionization cross section might be expected. The spectra of URu₂Si₂ were replotted from Ref. [14, 36], and bands α' , β' , and γ' in this figure correspond to band C, B (and E), and A (and D) in Fig. 2 of Ref. [36], respectively. The AIPES spectra obtained by integrating the ARPES spectra within $k_x = -2 - 2(\pi/a)$ and $k_y = 0 - 2(\pi/a)$ are shown in the right panel of each figure. The ARPES spectra are divided by the Fermi-Dirac function broadened by instrumental energy resolution to avoid the influences of Fermi cut-off. Sam-

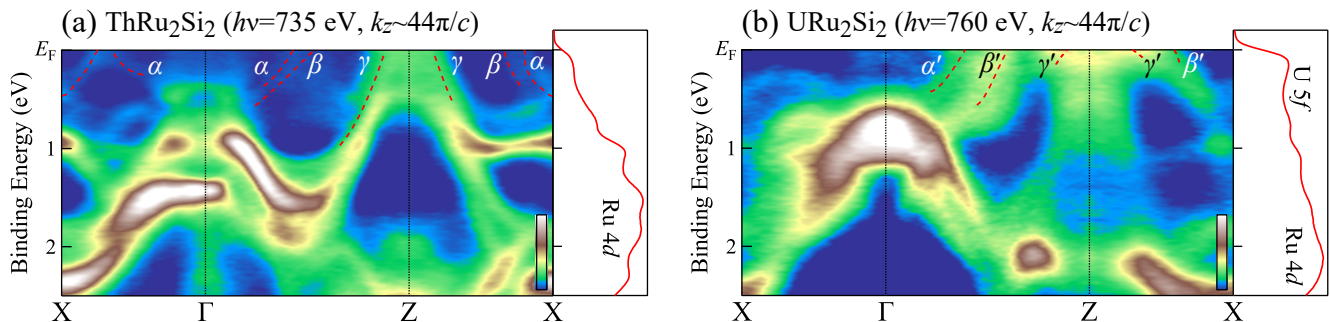


FIG. 7: (Online color) Comparison of ARPES spectra of ThRu_2Si_2 and URu_2Si_2 . The spectra are divided by the Fermi–Dirac function broadened by instrumental energy resolution to avoid the influences of Fermi cut-off. The AIPES spectra obtained by integrating the ARPES spectra within $k_x = -2 - 2(\pi/a)$ and $k_y = 0 - 2(\pi/a)$ are shown in the right panel of each figure. (a) ARPES spectra of ThRu_2Si_2 measured along the X – Γ – Z – X high-symmetry line at $h\nu = 735$ eV. (b) ARPES spectra of URu_2Si_2 measured along the X – Γ – Z – X high-symmetry line at $h\nu = 760$ eV. Data replotted from Ref. [14, 36], and bands α' , β' , and γ' in this figure correspond to band C, B (and E), and A (and D) in Fig. 2 of Ref. [36], respectively. Note that the bands α' , β' , and γ' should be renormalized in the very vicinity of E_F , but their behaviors are not well resolved due to the instrumental energy resolution.

ple temperature was $T = 20$ K, and both samples were in the paramagnetic phase.

The ARPES spectra of ThRu_2Si_2 and URu_2Si_2 have very similar structures, but there are many notable differences in their details. On the high-binding-energy side, the bands with large contributions from the Ru 4d states in the binding energy of $E_B = 0.5 - 2$ eV have similar cosine-shaped dispersions, but their details differ considerably. For example, the dispersion has enhanced intensity around the Γ point at $E_B \sim 1.5$ eV in ThRu_2Si_2 , while it is weak in URu_2Si_2 and the state at $E_B \sim 0.9$ eV is enhanced instead. The structure of the band around the Z point is also different between them. These suggest that the U 5f states are considerably hybridized with ligand states, and they substantially influence the entire band structure. This is in strong contrast with the case of CeRu_2Si_2 and LaRu_2Si_2 [15], where most of Ce 4f states are distributed on the high-binding-energy side as localized f^0 peak, and ARPES spectra are essentially identical except for the contribution of heavy quasi-particle bands located within $E_B \lesssim 0.2$ eV. This suggests that U 5f states are considerably hybridized with the ligand states in URu_2Si_2 while Ce 4f states are less hybridized in CeRu_2Si_2 .

More importantly, the structures in the vicinity of E_F are very different between ThRu_2Si_2 and URu_2Si_2 . The spectra of URu_2Si_2 have more complicated structures than those of ThRu_2Si_2 . One of the most prominent differences between these two sets of spectra is the dispersive features along the Γ –Z high-symmetry line. The intensity of bands α and β is very weak in the spectra of ThRu_2Si_2 , while the intensity of the corresponding bands α' and β' is significantly enhanced in the spectra of URu_2Si_2 . This suggests that bands α' and β' have large contributions from U 5f states, indicating the itinerant nature of U 5f states in URu_2Si_2 . Moreover, the spectral profiles in the very vicinity of E_F at the Z point

are also different between ThRu_2Si_2 and URu_2Si_2 . Band γ has relatively simple hole-like dispersion in ThRu_2Si_2 , while the corresponding band γ' exhibits more complex behavior just below E_F in URu_2Si_2 , suggesting that the hybridization is anisotropic in the momentum space. The strongly hybridized nature is consistent with the result of previous ARPES studies [12–14].

IV. CONCLUSION

The electronic structure of ThRu_2Si_2 was studied by AIPES and ARPES. The Th 4f core-level spectrum is very similar to that of Th metal, suggesting that Th is tetravalent in ThRu_2Si_2 . The three-dimensional shapes of the Fermi surfaces and the band structure were obtained experimentally by ARPES. Two hole-like Fermi surfaces around the Z point and one electron-like Fermi surface around the Γ point were observed, and the results are mostly consistent with the result of the dHvA study. The topology of the Fermi surface and the band structure of ThRu_2Si_2 were mostly explained by the band structure calculation. Meanwhile, the structure of the hole-pocket Fermi surface around the Z point was not well resolved, and the number of Fermi surfaces was not determined. Comparison of AIPES and ARPES spectra between ThRu_2Si_2 and URu_2Si_2 showed that they have very different natures especially in the vicinity of E_F . This indicates that the U 5f electrons in URu_2Si_2 are strongly hybridized with ligand states, suggesting that U 5f electrons in URu_2Si_2 have a considerably itinerant nature.

Acknowledgments

The experiments were performed under Proposal Nos. 2015A3810, 2015B3810, 2016A3810 and 2016B3810 at SPring-8 BL23SU. The present work was financially supported by JSPS KAKENHI Grant Numbers 21740271,

26400374, 16H01084 (J-Physics), and 16K05463; and Grants-in-Aid for Scientific Research on Innovative Areas “Heavy Electrons” (Nos. 20102002 and 20102003) from the Ministry of Education, Culture, Sports, Science, and Technology, Japan.

-
- * Present address: Department of Physics, University of Toyama, Toyama 930-8555, Japan
- [1] R. Hoffmann, *Solids and surfaces: a chemist's view of bonding in extended structures* (VCH Publishers, 1988).
- [2] M. Rotter, M. Tegel, and D. Johrendt, *Phys. Rev. Lett.* **101**, 107006 (2008).
- [3] F. Steglich, J. Aarts, C. D. Bredl, W. Lieke, D. Meschede, W. Franz, and H. Schäfer, *Phys. Rev. Lett.* **43**, 1892 (1979).
- [4] M. Besnus, J. Kappler, P. Lehmann, and A. Meyer, *Solid State Commun.* **55**, 779 (1985).
- [5] O. Trovarelli, C. Geibel, S. Mederle, C. Langhammer, F. M. Grosche, P. Gegenwart, M. Lang, G. Sparn, and F. Steglich, *Phys. Rev. Lett.* **85**, 626 (2000).
- [6] O. Stockert, S. Kirchner, F. Steglich, and Q. Si, *J. Phys. Soc. Jpn.* **81**, 011001 (2012).
- [7] F. Steglich, J. Arndt, O. Stockert, S. Friedemann, M. Brando, C. Klingner, C. Krellner, C. Geibel, S. Wirth, S. Kirchner, and Q. Si, *Journal of Physics: Condensed Matter* **24**, 294201 (2012).
- [8] T. T. M. Palstra, A. A. Menovsky, J. v. d. Berg, A. J. Dirkmaat, P. H. Kes, G. J. Nieuwenhuys, and J. A. Mydosh, *Phys. Rev. Lett.* **55**, 2727 (1985).
- [9] J. A. Mydosh and P. M. Oppeneer, *Rev. Mod. Phys.* **83**, 1301 (2011).
- [10] J. Mydosh and P. Oppeneer, *Philos. Mag.* **94**, 3642 (2014).
- [11] A. F. Santander-Syro, M. Klein, F. L. Boariu, A. Nuber, P. Lejay, and F. Reinert, *Nat. Phys.* **5**, 637 (2009).
- [12] T. Durakiewicz, *Philos. Mag.* **94**, 3723 (2014).
- [13] S.-i. Fujimori, *J. Phys.: Condens. Matter* **28**, 153002 (2016).
- [14] S.-i. Fujimori, Y. Takeda, T. Okane, Y. Saitoh, A. Fujimori, H. Yamagami, Y. Haga, E. Yamamoto, and Y. Ōnuki, *J. Phys. Soc. Jpn.* **85**, 062001 (2016).
- [15] J. Denlinger, G.-H. Gweon, J. Allen, C. Olson, M. Maple, J. Sarrao, P. Armstrong, Z. Fisk, and H. Yamagami, *J. Electron Spectrosc. Relat. Phenom.* **117-118**, 347 (2001).
- [16] Y. Matsumoto, Y. Haga, N. Tateiwa, H. Aoki, N. Kimura, T. D. Matsuda, E. Yamamoto, Z. Fisk, and H. Yamagami, *JPS Conf. Proc.* **3**, 011096 (2014).
- [17] Y. Matsumoto, Y. Haga, N. Tateiwa, H. Aoki, N. Kimura, T. Yamamura, E. Yamamoto, T. D. Matsuda, Z. Fisk, and H. Yamagami, *J. Phys. Soc. Jpn.* **85**, 104709 (2016).
- [18] Y. Haga, Y. Matsumoto, N. Tateiwa, E. Yamamoto, N. Kimura, T. Yamamura, and Z. Fisk, *J. Phys. Conf. Ser.* **592**, 012036 (2015).
- [19] N. Emi, R. Hamabata, D. Nakayama, T. Miki, T. Koyama, K. Ueda, T. Mito, Y. Kohori, Y. Matsumoto, Y. Haga, E. Yamamoto, Z. Fisk, and N. Tsujii, *J. Phys. Soc. Jpn.* **84**, 063702 (2015).
- [20] A. Yokoya, T. Sekiguchi, Y. Saitoh, T. Okane, T. Nakatani, T. Shimada, H. Kobayashi, M. Takao, Y. Teraoka, Y. Hayashi, S. Sasaki, Y. Miyahara, T. Harami, and T. A. Sasaki, *J. Synchrotron Rad.* **5**, 10 (1998).
- [21] Y. Saitoh, Y. Fukuda, Y. Takeda, H. Yamagami, S. Takahashi, Y. Asano, T. Hara, K. Shirasawa, M. Takeuchi, T. Tanaka, and H. Kitamura, *J. Synchrotron Rad.* **19**, 388 (2012).
- [22] D. V. Vyalikh, S. Danzenbacher, C. Krellner, K. Kummer, C. Geibel, Y. Kucherenko, C. Laubschat, M. Shi, L. Patthey, R. Follath, and S. L. Molodtsov, *J. Electron Spectrosc. Relat. Phenom.* **181**, 70 (2010).
- [23] S.-i. Fujimori, T. Ohkochi, I. Kawasaki, A. Yasui, Y. Takeda, T. Okane, Y. Saitoh, A. Fujimori, H. Yamagami, Y. Haga, E. Yamamoto, and Y. Ōnuki, *Phys. Rev. B* **91**, 174503 (2015).
- [24] S.-i. Fujimori, T. Ohkochi, I. Kawasaki, A. Yasui, Y. Takeda, T. Okane, Y. Saitoh, A. Fujimori, H. Yamagami, Y. Haga, E. Yamamoto, Y. Tokiwa, S. Ikeda, T. Sugai, H. Ohkuni, N. Kimura, and Y. Ōnuki, *J. Phys. Soc. Jpn.* **81**, 014703 (2012).
- [25] O. Gunnarsson, K. Schönhammer, D. D. Sarma, F. U. Hillebrecht, and M. Campagna, *Phys. Rev. B* **32**, 5499 (1985).
- [26] D. D. Sarma, F. U. Hillebrecht, O. Gunnarsson, and K. Schönhammer, *Z. Phys. B* **63**, 305 (1986).
- [27] Y. Baer, in *Handbook on the Physics and Chemistry of the Actinides. Vol. 1* (North-Holland, Amsterdam, 1984), vol. 1, chap. 4, p. 271.
- [28] B. Johansson, R. Ahuja, O. Eriksson, and J. M. Wills, *Phys. Rev. Lett.* **75**, 280 (1995).
- [29] S. Friedemann, S. Wirth, N. Oeschler, C. Krellner, C. Geibel, F. Steglich, S. MaQuilon, Z. Fisk, S. Paschen, and G. Zwicky, *Phys. Rev. B* **82**, 035103 (2010).
- [30] W. Eberhardt and E. W. Plummer, *Phys. Rev. B* **21**, 3245 (1980).
- [31] S.-i. Fujimori, T. Ohkochi, T. Okane, Y. Saitoh, A. Fujimori, H. Yamagami, Y. Haga, E. Yamamoto, and Y. Ōnuki, *Phys. Rev. B* **86**, 235108 (2012).
- [32] S.-i. Fujimori, I. Kawasaki, A. Yasui, Y. Takeda, T. Okane, Y. Saitoh, A. Fujimori, H. Yamagami, Y. Haga, E. Yamamoto, and Y. Ōnuki, *Phys. Rev. B* **89**, 104518 (2014).
- [33] H. Daimon, S. Imada, H. Nishimoto, and S. Suga, *J. Electron Spectrosc. Relat. Phenom.* **76**, 487 (1995).
- [34] M. Kobata, S.-i. Fujimori, Y. Takeda, T. Okane, Y. Saitoh, K. Kobayashi, H. Yamagami, A. Nakamura, M. Hedo, T. Nakama, and Y. Ōnuki, *J. Phys. Soc. Jpn.* **85**, 094703 (2016).
- [35] P. Zhang, P. Richard, T. Qian, Y.-M. Xu, X. Dai, and H. Ding, *Rev. Sci. Instrum.* **82**, 043712 (2011).
- [36] I. Kawasaki, S.-i. Fujimori, Y. Takeda, T. Okane, A. Ya-

- sui, Y. Saitoh, H. Yamagami, Y. Haga, E. Yamamoto,
and Y. Ōnuki, Phys. Rev. B **83**, 235121 (2011).
[37] V. Strocov, J. Electron Spectrosc. Relat. Phenom. **130**,
65 (2003).